Comparative Analysis of Essential Collective Dynamics and NMR-Derived Flexibility Profiles in Evolutionarily Diverse Prion Proteins

Kolattukudy P. Santo [1,2], Mark Berjanskii[3], David S. Wishart[1,4], and Maria Stepanova[1]

(1) – National Institute for Nanotechnology NRC, Edmonton, Alberta, Canada;

(2) – Department of Electrical and Computer Engineering, University of Alberta, Edmonton, Canada;

(3) – Department of Computing Sciences, University of Alberta, Edmonton, Canada;

(4) – Department of Biological Sciences, University of Alberta, Edmonton, Canada

Abstract

Collective motions on ns-μs time scales are known to have a major impact on protein folding, stability, binding and enzymatic efficiency. It is also believed that these motions may have an important role in the early stages of prion protein misfolding and prion disease. In an effort to accurately characterize these motions and their potential influence on the misfolding and prion disease transmissibility we have conducted a combined analysis of molecular dynamic simulations and NMR-derived flexibility measurements over a diverse range of prion proteins. Using a recently developed numerical formalism, we have analyzed the essential collective dynamics (ECD) for prion proteins from 8 different species including human, cow, elk, cat, hamster, chicken, turtle and frog. We also compared the numerical results with flexibility profiles generated by the random coil index (RCI) from NMR chemical shifts. Prion protein backbone flexibility derived from experimental NMR data and from theoretical computations show strong agreement with each other, demonstrating that it is possible to predict the observed RCI profiles employing the numerical ECD formalism. Interestingly, flexibility differences in the loop between second beta strand (S2) and the second alpha helix (HB) appear to distinguish prion proteins from species that are susceptible to prion disease and those that are resistant. Our results show that the different levels of flexibility in the S2-HB loop in various species are predictable via the ECD method, indicating that ECD may be used to identify disease resistant variants of prion proteins, as well as the influence of prion proteins mutations on disease susceptibility or misfolding propensity.

Contents

Figures S1-S16 below present the dynamical domains and flexibility profiles for elk, bovine, cat, hamster, human, frog, turtle, and chicken, obtained from independent MD trajectories different from those considered in the main article. Figures S1, S3, S5, S7, S9, S11, S13, and S15 show the dynamical domains, and figures S2, S4, S6, S8, S10, S12, S14, and S16 show the flexibility profiles. Figure S17 illustrates sequence alignment of the species considered.

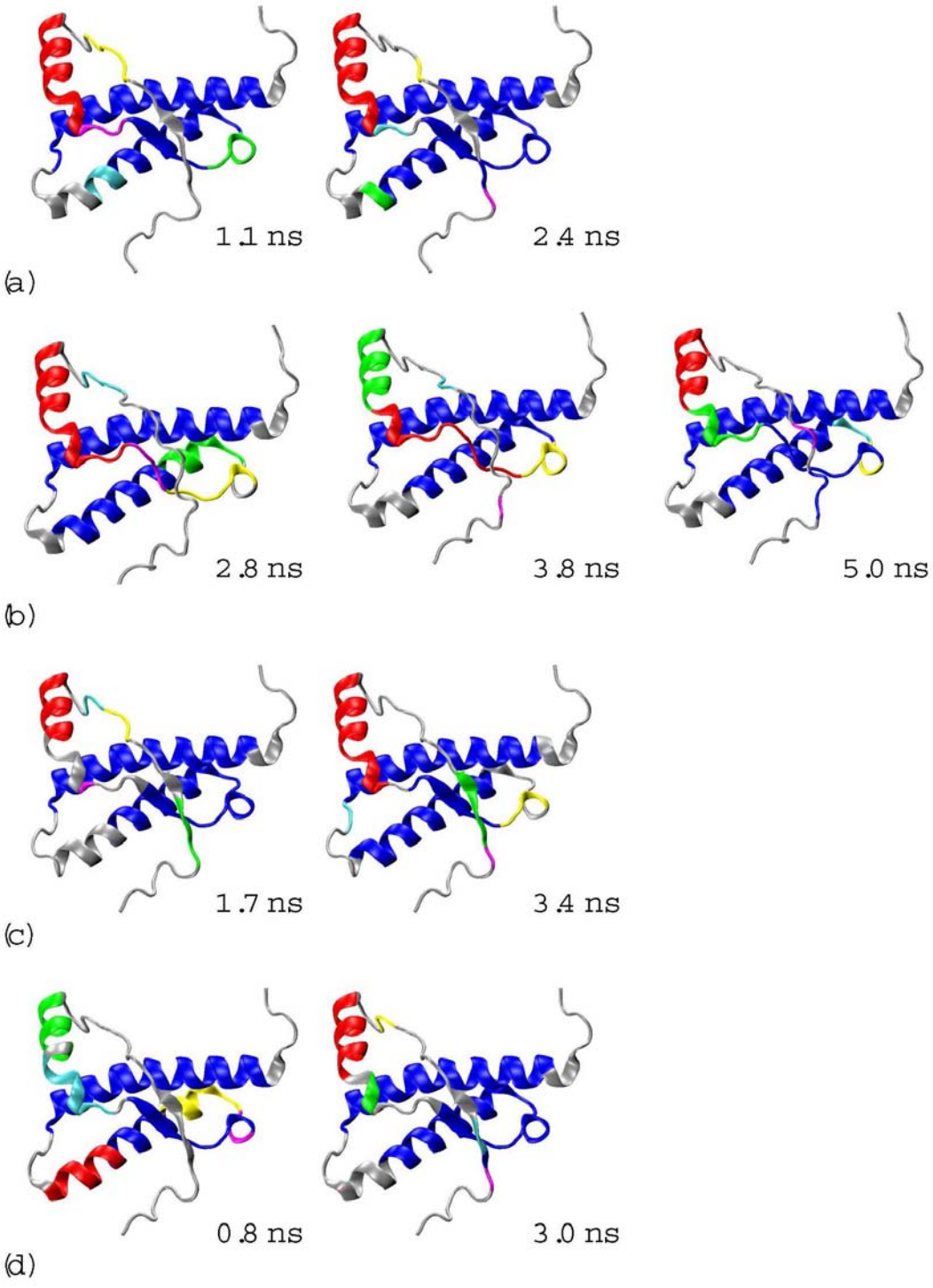

Figure S1. Dynamical domains for elk prion protein identified from four different MD trajectories denoted by (a), (b), (c), and (d), respectively, at times indicated by the subscripts. Six largest domains are shown with the largest domain colored blue and the smaller domains colored red, green, yellow, cyan, and magenta in the order of the decreasing size.

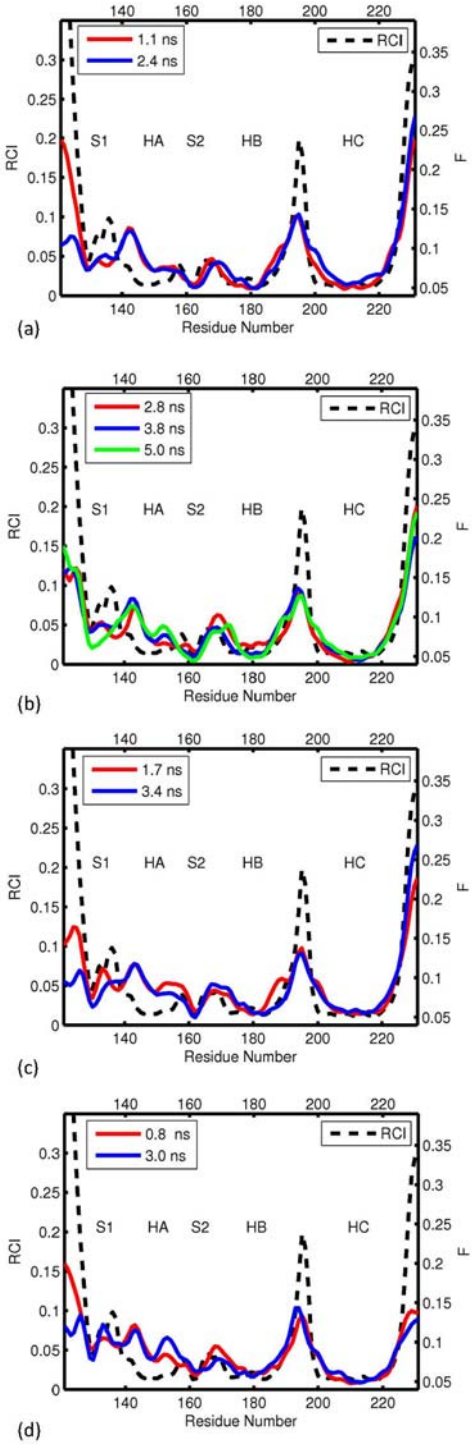

Figure S2. Computed flexibility profiles for elk prion protein identified from four MD trajectories denoted by (a), (b), (c), and (d), respectively, at times indicated in the legend boxes, overimposed on the experimental RCI profile shown by black dashed curve.

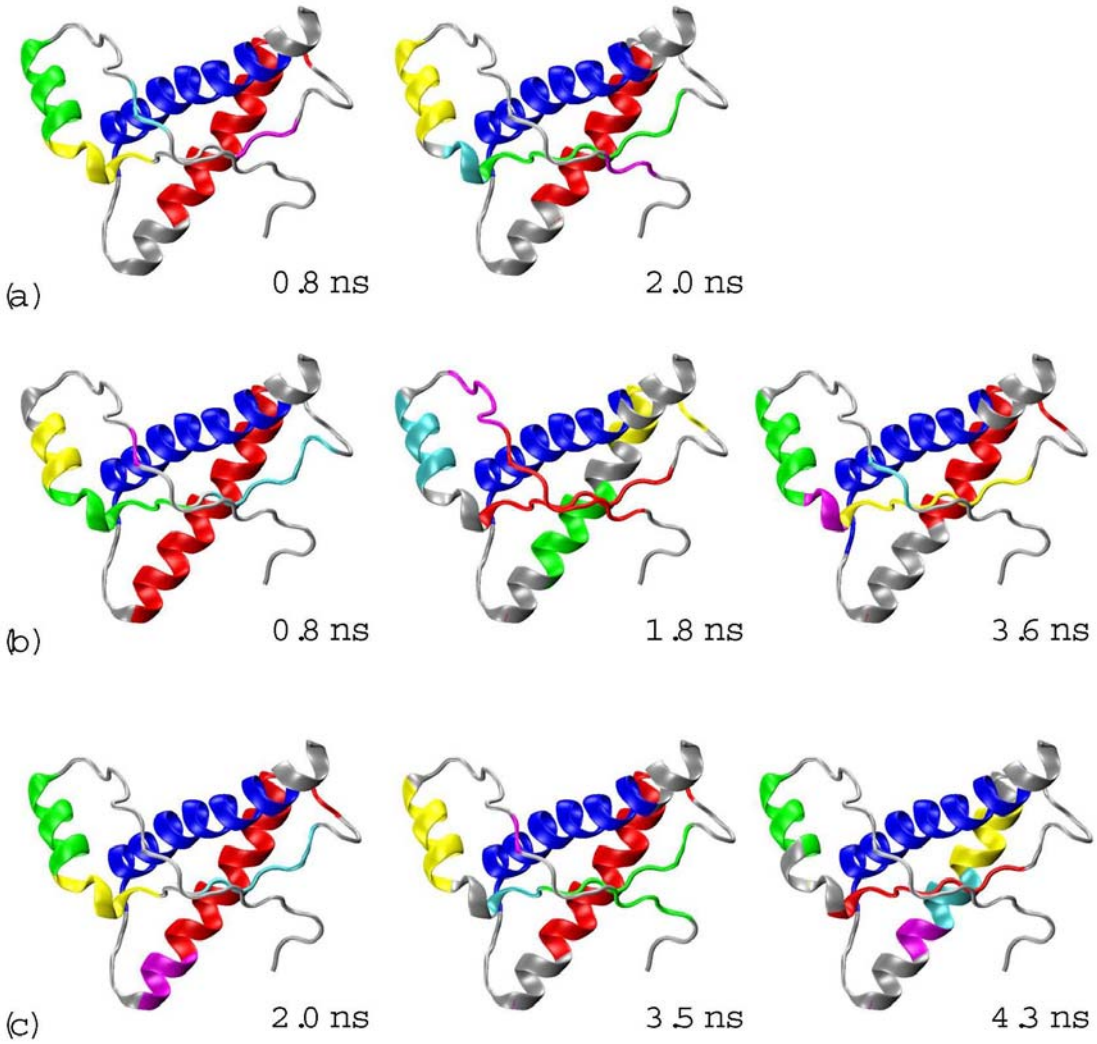

Figure S3. Dynamical domains for bovine prion protein identified from three MD trajectories denoted by (a), (b) and (c) respectively, at times indicated by the subscripts. The meaning of colors is as in Figure S1.

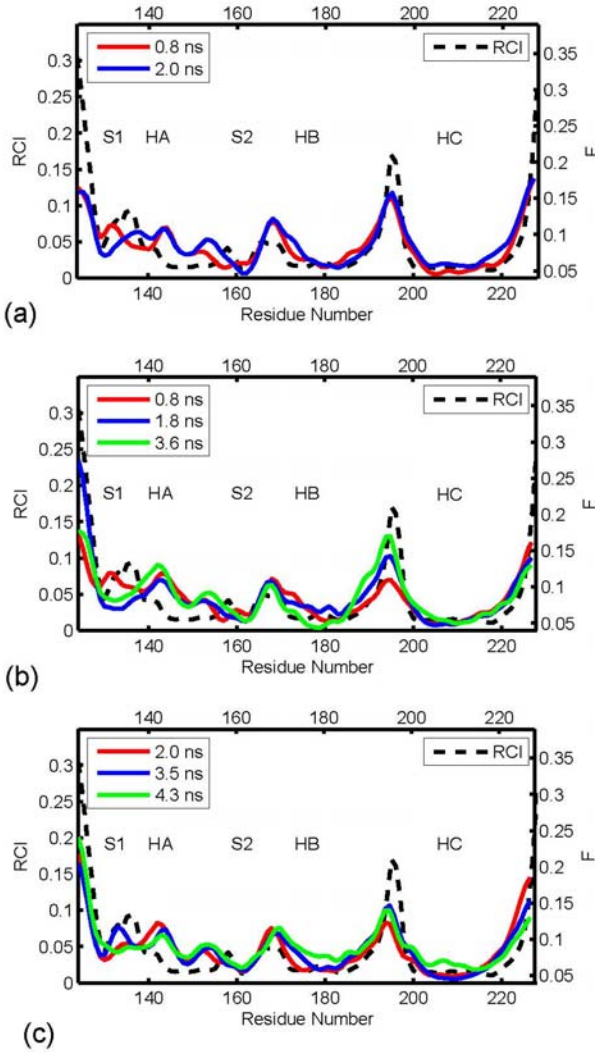

Figure S4. Computed flexibility profiles for bovine prion protein identified from three MD trajectories denoted by (a), (b) and (c), respectively, at times indicated in the legend boxes, overimposed on the experimental RCI profile shown by black dashed curve.

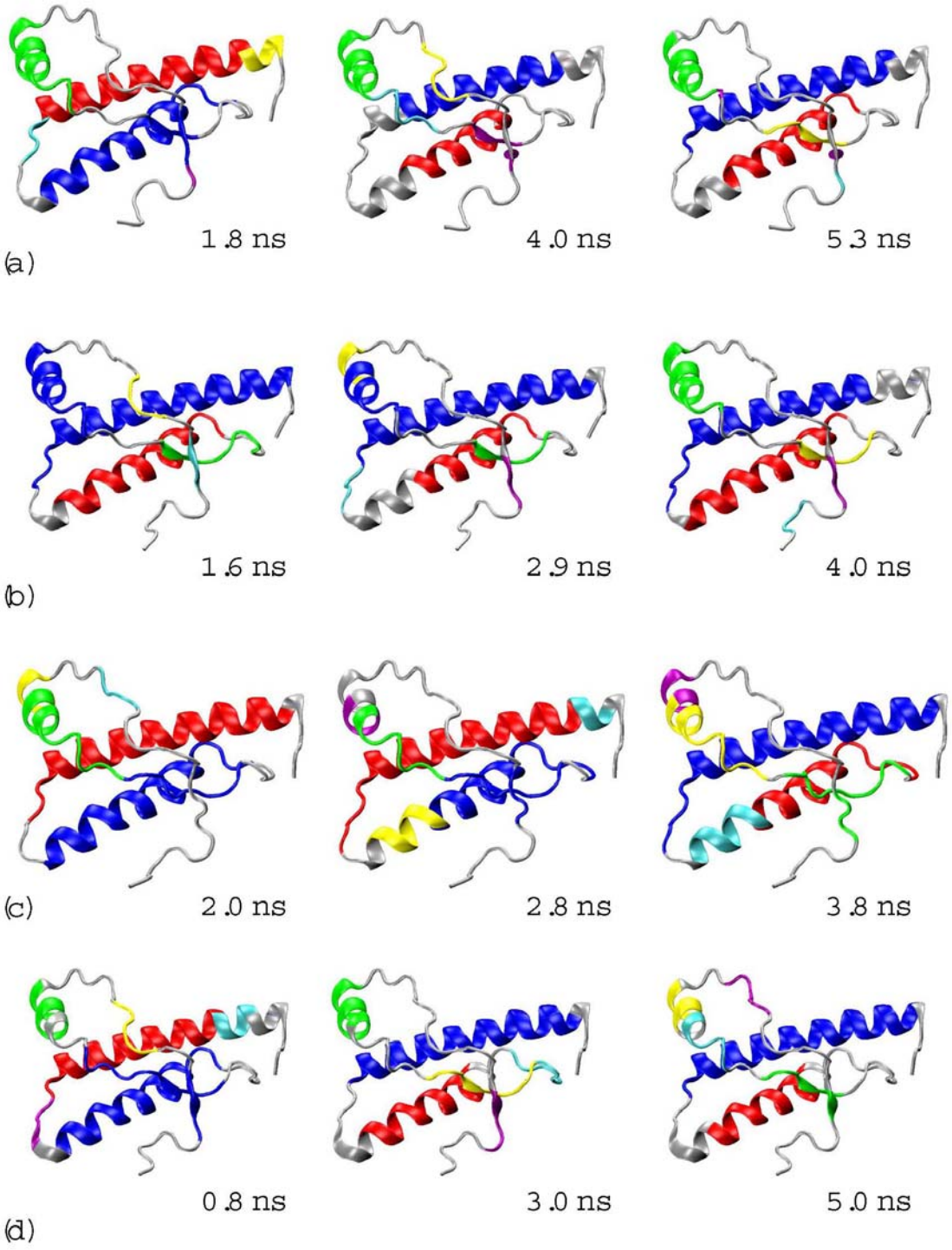

Figure S5. Dynamical domains for cat prion protein identified from four different MD trajectories denoted by (a), (b), (c), and (d), respectively, at times indicated by the subscripts.

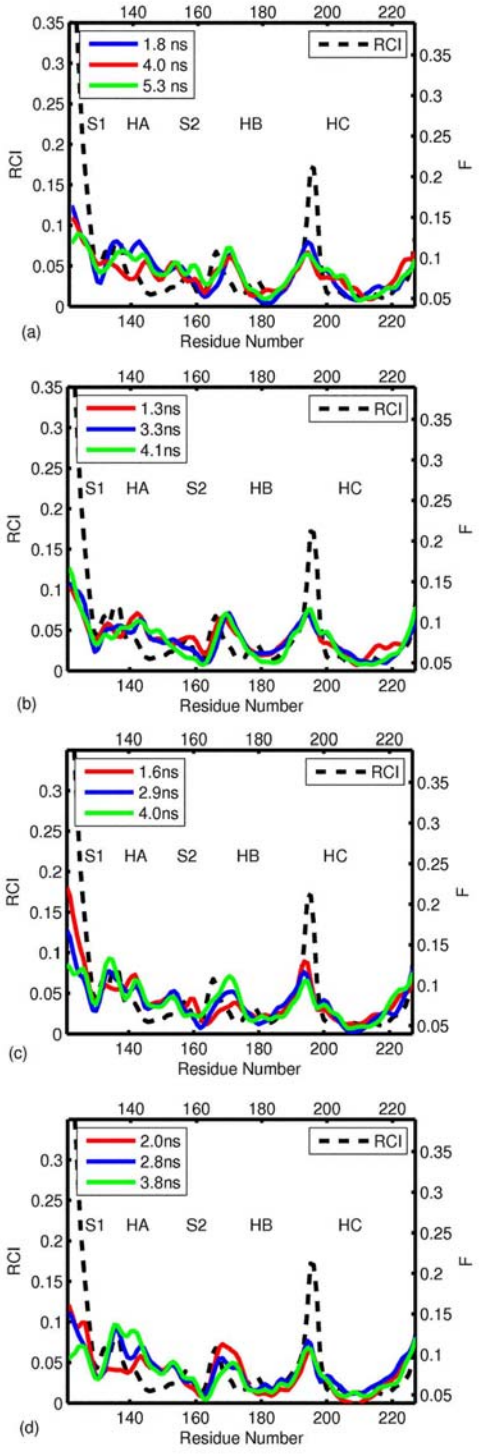

Figure S6. Computed flexibility profiles for cat prion protein identified from four MD trajectories denoted by (a), (b), (c), and (d), respectively, at times indicated in the legend boxes, overimposed on the experimental RCI profile shown by black dashed curve.

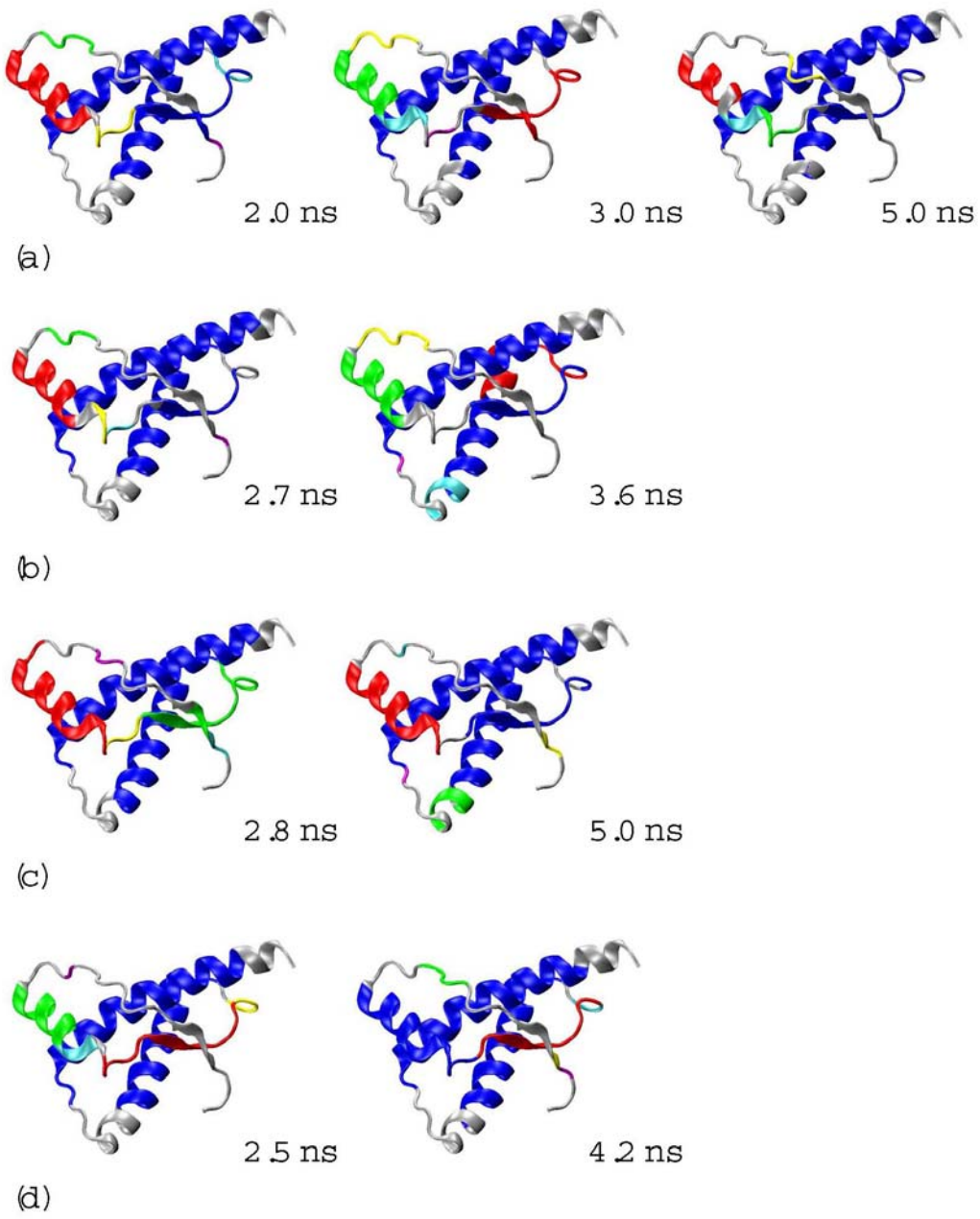

Figure S7. Dynamical domains for hamster prion protein identified from four different MD trajectories denoted by (a), (b), (c), and (d), respectively, at times indicated by the subscripts.

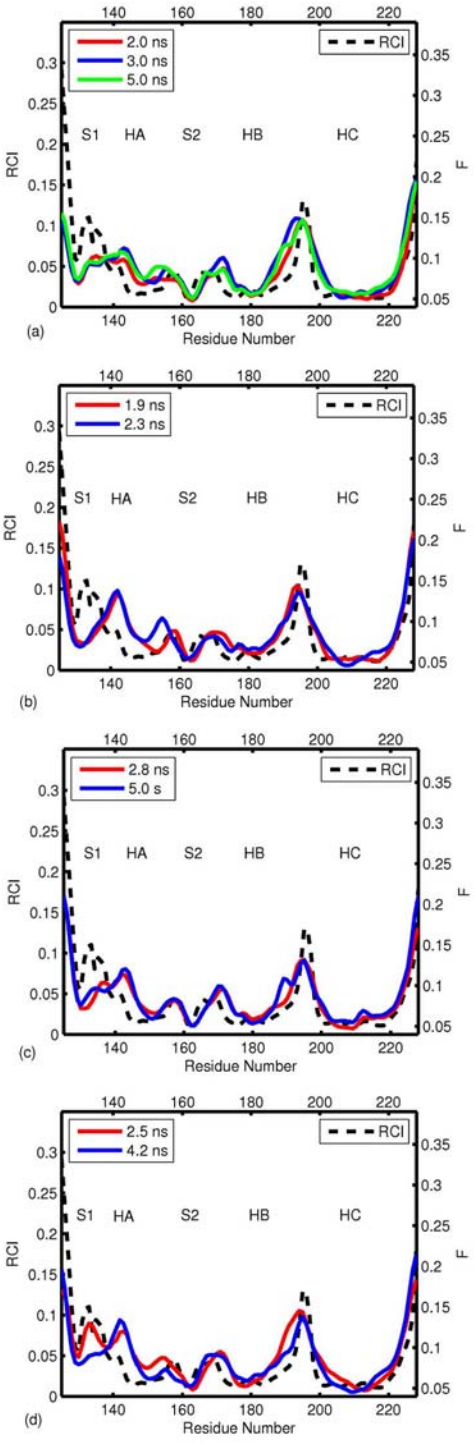

Figure S8. Computed flexibility profiles for hamster prion protein identified from four MD trajectories denoted by (a), (b), (c), and (d), respectively, at times indicated in the legend boxes, overimposed on the experimental RCI profile shown by black dashed curve.

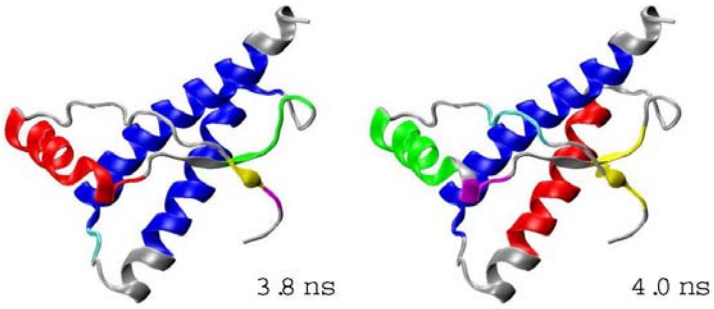

Figure S9. Dynamical domains for human prion protein identified from a MD trajectory at times indicated by the subscripts.

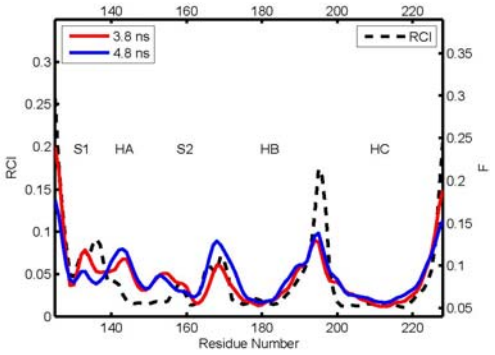

Figure S10. Computed flexibility profiles for human prion protein identified from a MD trajectory at times indicated in the legend boxes, overimposed on the experimental RCI profile shown by black dashed curve.

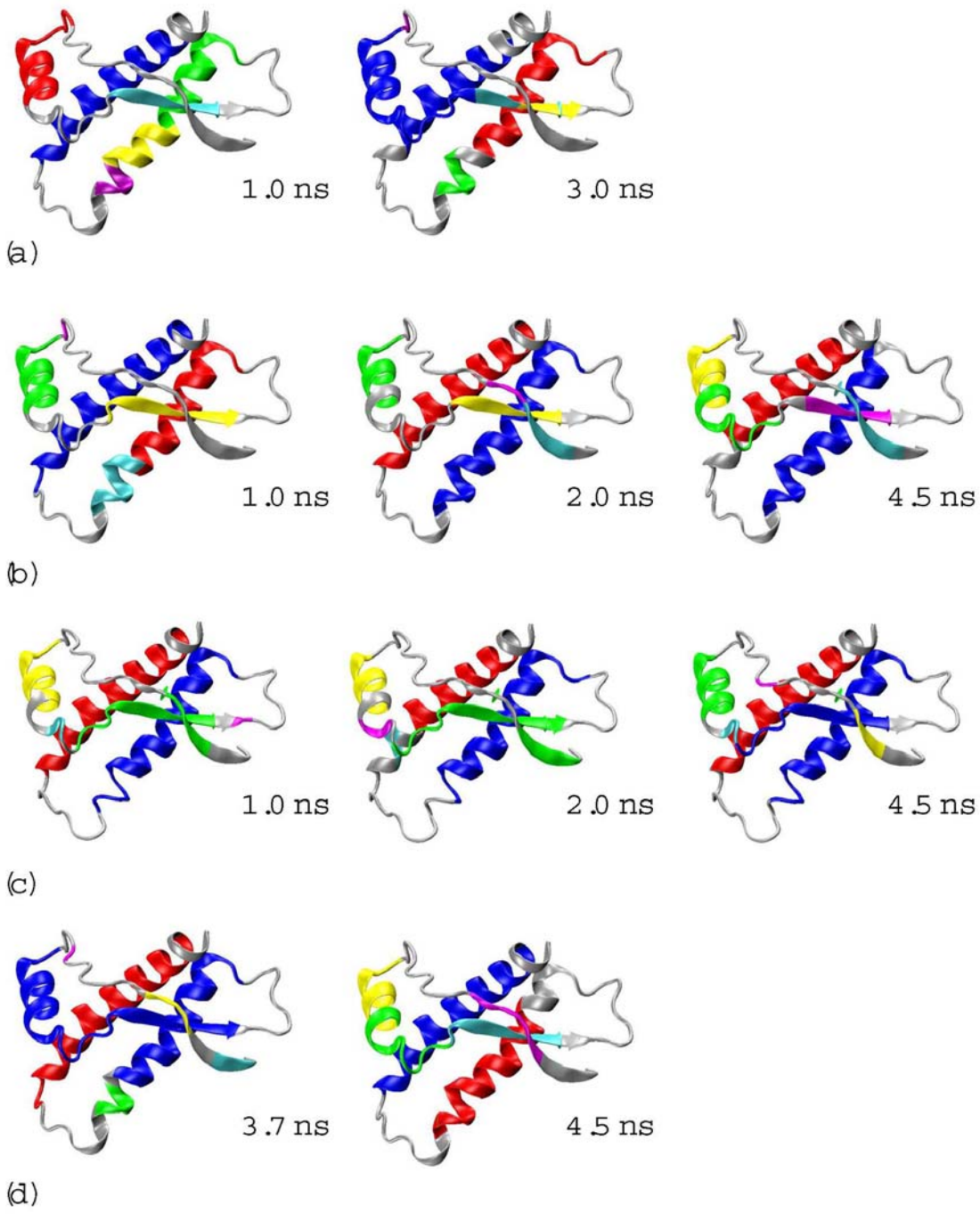

Figure S11. Dynamical domains for frog prion protein identified from four different MD trajectories denoted by (a), (b), (c), and (d), respectively, at times indicated by the subscripts.

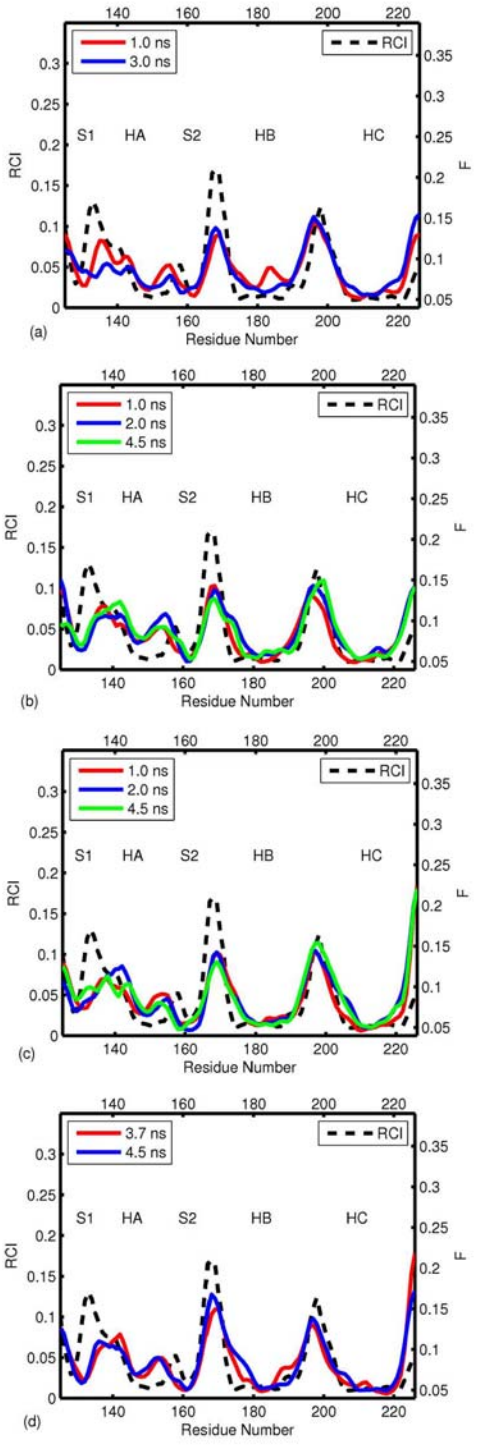

Figure S12. Computed flexibility profiles for frog prion protein identified from four MD trajectories denoted by (a), (b), (c), and (d), respectively, at times indicated in the legend boxes, overimposed on the experimental RCI profile shown by black dashed curve.

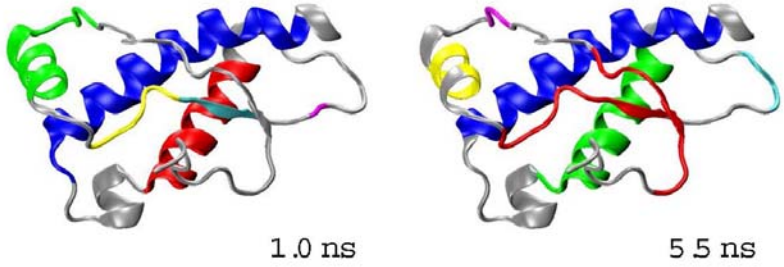

Figure S13. Dynamical domains for turtle prion protein identified from a MD trajectory at times indicated by the subscripts.

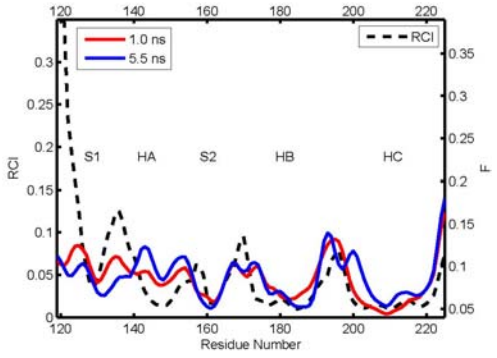

Figure S14. Computed flexibility profiles for turtle prion protein identified from a MD trajectory at times indicated in the legend boxes, overimposed on the experimental RCI profile shown by black dashed curve.

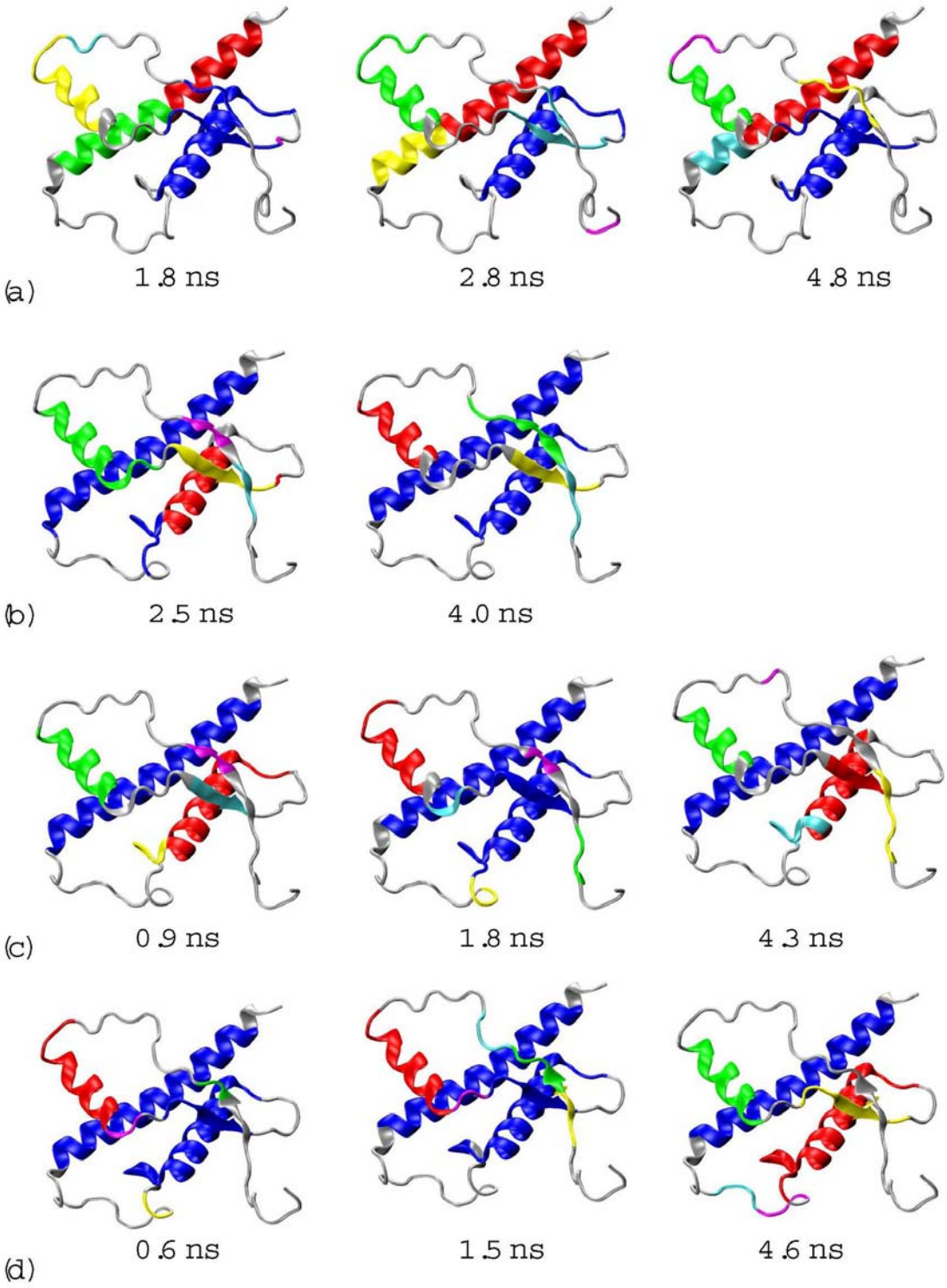

Figure S15. Dynamical domains for chicken prion protein identified from four different MD trajectories denoted by (a), (b), (c), and (d), respectively, at times indicated by the subscripts.

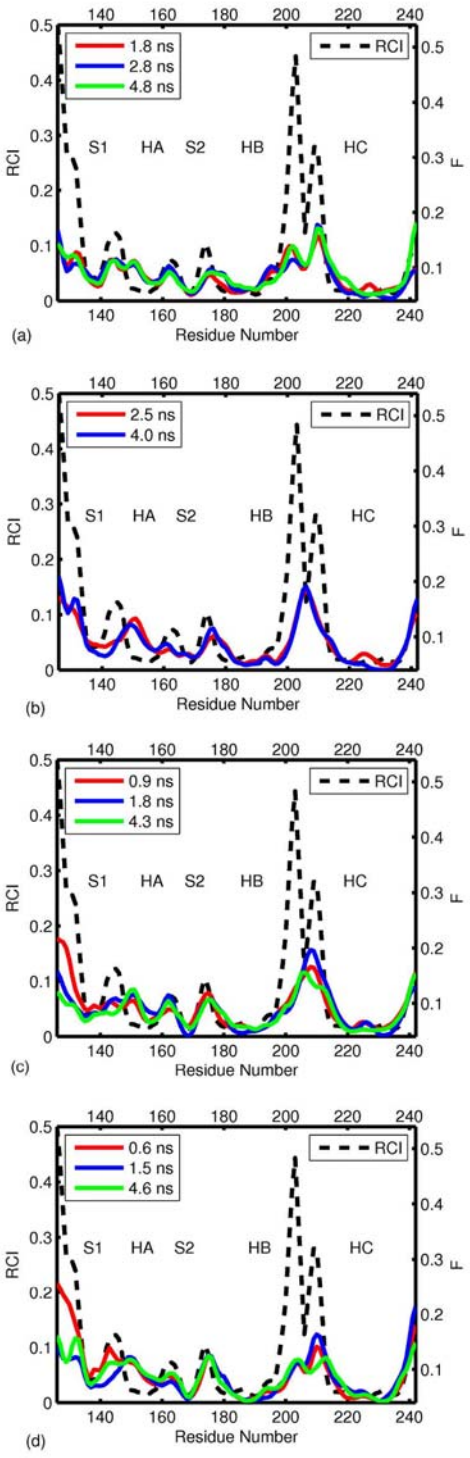

Figure S16. Computed flexibility profiles for chicken prion protein identified from four MD trajectories denoted by (a), (b), (c), and (d), respectively, at times indicated in the legend boxes, overimposed on the experimental RCI profile shown by black dashed curve.

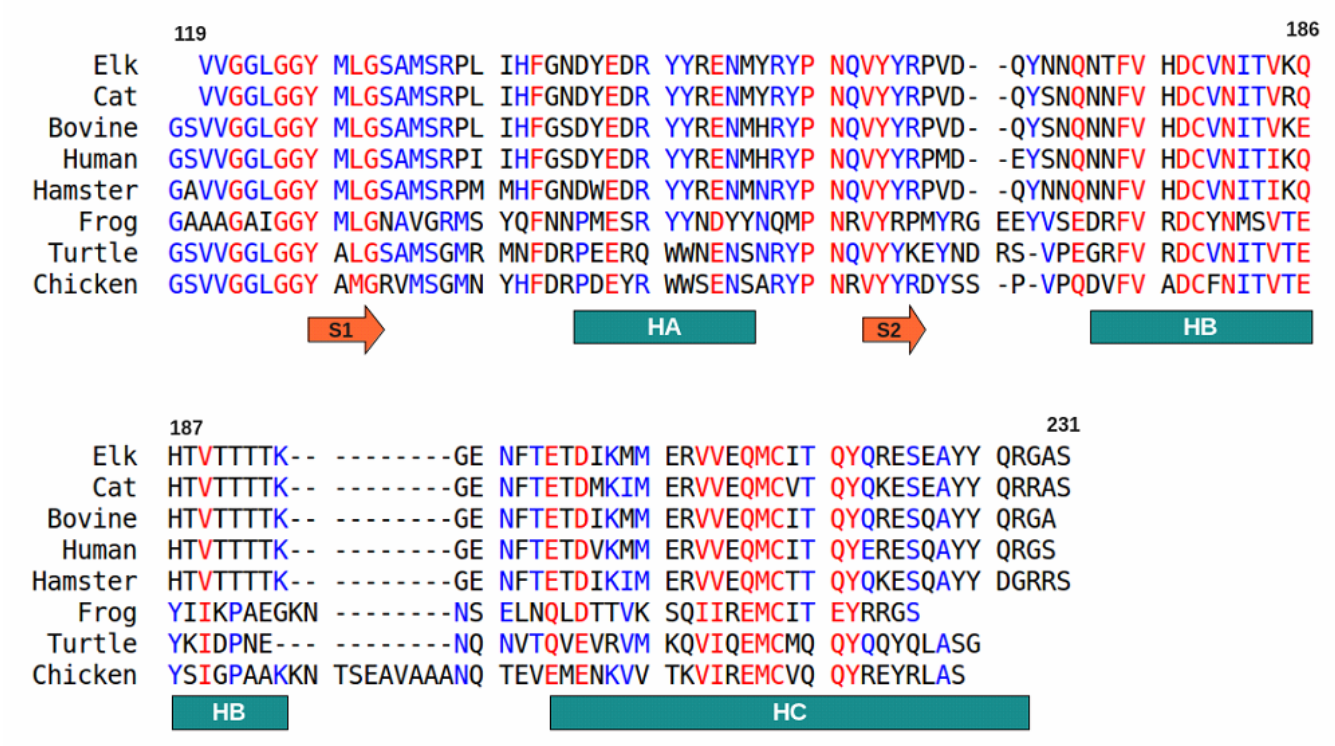

Figure S17. Sequence alignment of PrP C-terminal domains that correspond to PDB entries in Table 1. Residues with high consensus level (>90% conservation) and low consensus level (>50% and <90% conservation) are colored red and blue, respectively. The span of secondary structure elements is shown underneath the alignment. β-strands are shown as orange arrows and helices are shown as teal rectangles. Numbers of the first and the last residue on each alignment panel are shown. Residue numbering corresponds to PDB file of human prion protein (1QM3). Residues prior to position 119, if any, have been removed from primary sequences. The figure has been generated with Multalin [Corpet F. Multiple sequence alignment with hierarchical clustering. *Nucleic Acids Res* 1988; 16: 10881-10890] and Microsoft Power Point.